NASA/CR-97- 206141

COLLEGE OF ENGINEERING
THE UNIVERSITY OF TEXAS AT AUSTIN

Robotics Research Center • PRC: Mail Code R9925 • Austin, Texas 78712-1100
Telephone (512) 471-3039 • FAX (512) 471-3987

April 16, 1997

Mr. John Chladek
M.S. ER6
NASA - Johnson Space Center
2101 NASA Road 1
Houston, TX 77058

Dear John:

The enclosed is a compact summary of the work done under Grant NAG9-411 ~~NAG-11~~. This has been wonderful support for the University and I very much appreciate your role and others at JSC in giving us good advice and direction. As you can see from the table of contents, the program has covered a very broad range of topics. The 15 technical reports are those which were directly supported by the grant. Note also. that 13 M.Sc. and 11 Ph.D. students have also been directly involved in this effort. Finally, four staff members (Tesar, Tosunoglu, Hooper, and Freeman) have been involved and participated in the direction of the research.

Note, that we believe the brake development could be considered as patentable. A brief summary report is enclosed for your review.

John, we appreciate JSC's interest in our program. We hope it will continue at an expanded level in the future.

Sincerely yours,

Delbert Tesar

Delbert Tesar, P.E., Ph.D.
Carol Cockrell Curran Chair in Engineering

DT/jt
Enclosures
xc: Ms. Kathy Bradley, Engineering Business Mgmt. Office

Table of Contents

	Topic	Page
i.	Table of Contents	2
I.	Introduction	3
II.	Hardware	3
II-A.	Dual-Actuator	3
II-B.	Knuckle Fault-Tolerance Test-Bed	4
II-C.	Digital Integrated Servo Controller (DISC)	5
III.	Software	7
III-A.	Multi-Criteria Decision Making for Configuration Management	7
III-B.	Dual-Arm Control	8
IV.	Theoretical	9
IV-A.	Performance Criteria	9
IV-B.	Technical Reports	14
IV-C.	List of Graduates from Program	16

List of Figures

	Title	Page
1.	Dual-Actuator on Test-Stand	3
2.	4-legged Platform Module	4
3.	Knuckle Under Test	4
4.	Photograph of the DISC	5
5.	Hypercube for 3 Extra DOF	8
6.	6 Axis Wrist Transformations	8
7.	21 DOF Serpentine Robot	8
8.	Maintains Path After Fault	8
9.	Robot Handling Thin Plate	9
10.	17 DOF Dual-Arm Robot	9

I. Introduction

This report describes work developing fault tolerant redundant robotic architectures and adaptive control strategies for robotic manipulator systems which can dynamically accommodate drastic robot manipulator mechanism, sensor or control failures and maintain stable end-point trajectory control with minimum disturbance. Kinematic designs of redundant, modular, reconfigurable arms for fault tolerance were pursued at a fundamental level. The approach developed robotic testbeds to evaluate disturbance responses of fault tolerant concepts in robotic mechanisms and controllers. The development was implemented in various fault tolerant mechanism testbeds including duality in the joint servo motor modules, parallel and serial structural architectures, and dual arms. All have real-time adaptive controller technology to react to mechanism or controller disturbances (failures) to perform real-time reconfiguration to continue the task operations. The developments fall into three main areas: hardware, software, and theoretical.

II. Hardware

II-A. Dual Actuator

Existing drive systems usually include motor, encoder (or resolver), brake, drive train and joint bearings. They have no fault tolerance capability and could suffer failure through a variety of modes. To provide fault tolerance, one option suggested at NASA-JSC is to use multiple motors driving separate primary gears in a common gear box. This requires that all motors be capable of rotation at all times and any degradation in a motor's performance affects the joint. Another option uses dual motors driving a common axis through a bevel differential drive. This work suggests that such a drive system should have a high forward efficiency and low backdrive efficiency. Though this design can tolerate a failure of either motor, a failure in the differential will cripple the joint. Without complete functional duality, it is impossible to mask all the probable failure modes. It is, therefore, imperative that a dual actuator set driving a single joint be designed.

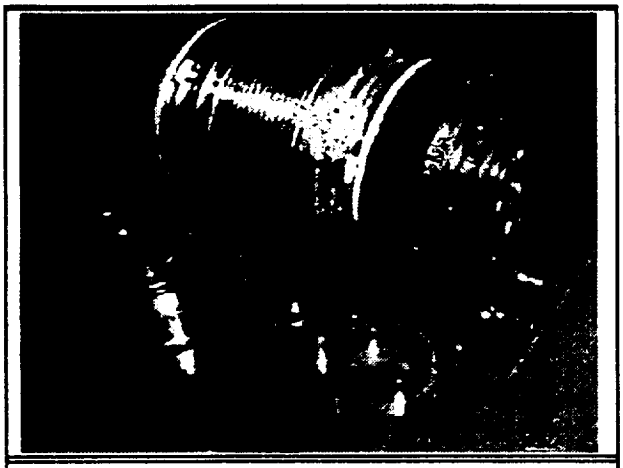

Figure 1. Dual-Actuator on Test-Stand

Parameter	Value
torque	800 Nm
reduction	30:1
diameter	.2 m
length	.3 m
weight	450 N
stiffness	$10*10^6$ Nm
power	1.5 Hp

Table 1. Parameters of the Dual-Actuator

Figure 1. shows a photograph of the actual module on its test-stand. It is symmetrical about the center line and has complete duality between the right and left halves. Each half contains an armature, rare earth magnets, resolvers, brakes and Ferguson's paradox epicyclic gear trains. The Ferguson's paradox gear train was chosen primarily for its high gear ratio and compactness. The module has attributes of low-weight, high-stiffness, minimal interfaces to the system controller, and overall compactness. The prototype of the module incorporates mainly off-the-shelf components compactly laid out in a configuration that provides low weight and high drive stiffness. Table 1. lists some of the performance

characteristics of the module. The dual sided module provides fault tolerance in the event of failure of one side by "doubling up" on the other side by peaking its power for a short period of time. In the event of seizure, the failed side has to be detached from the power train to allow the joint to turn. For the prototype actuator, such a detachment is necessary even in the case when the failed motor is free to move because of the non-backdrivability of Ferguson's paradox gear trains. Conceptually, a dual fault tolerant actuator can be incorporated into fault tolerance at levels II, III, and IV. The prototype module, however, is designed for testing and development as a stand-alone unit and is mounted to a heavy steel test stand.

II-B. Knuckle Fault-Tolerance Testbed

The knuckle is designed to tolerate a minimum of 1 fault before failing. The system controller acts as a supervisor in analyzing the sensory feedback with a Fault Detection and Isolation (FDI) algorithm to determine if a fault has occurred in the knuckle. If a fault occurs at the actuator level, the motor is removed by disengaging a clutch. Each servo system consists of a clutch, a brushless resolver, a brake, Hall-effect sensors, and a three-phase Brushless DC motor. Each motor has a peak torque rating of 40 Newton*meters and a continuous rating of 6 Newton*meters. There is a .5 meter spacing between the output shafts of the motors, measured along the common axis of rotation. The entire knuckle system weighs about 440 Newtons. Each motor is controlled by a Digital Integrated Servo Controller (DISC). The system controller is a personal computer operating under the Lynx O/S® real-time operating system.

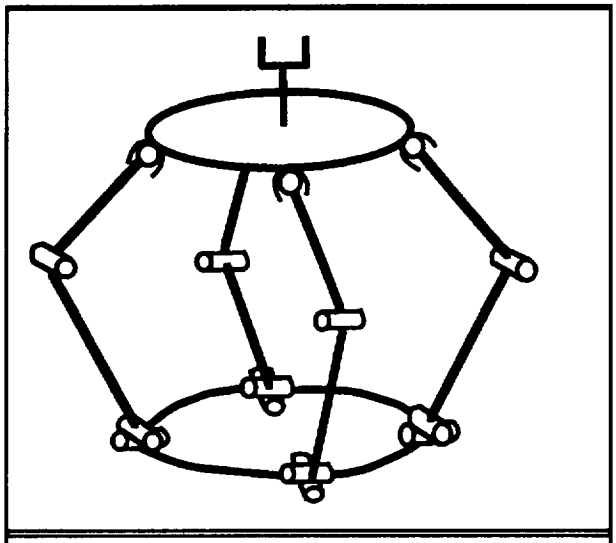

Figure 2. 4-legged Platform Module

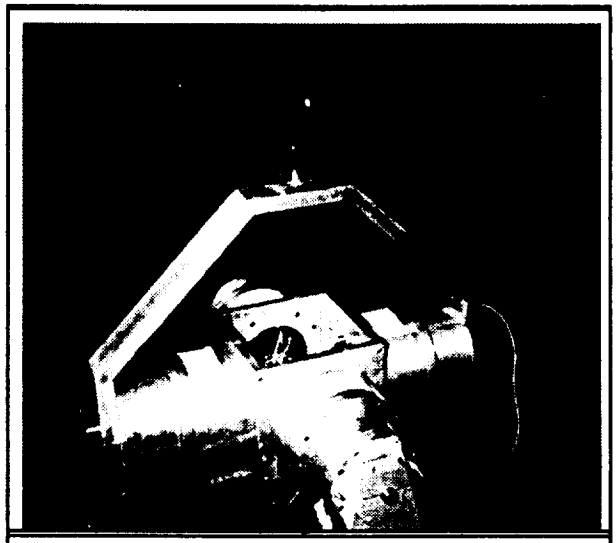

Figure 3. Knuckle Under Test

An FDI algorithm supervises the servo systems. The topic of FDI enjoys a rich history in the literature. Roughly twenty years ago Willsky generated a survey paper presenting a number of statistical techniques for fault detection in dynamic systems. Over ten years ago Isermann developed another survey paper on fault detection based on modeling and estimation methods. NASA also has shown considerable work in the area of FDI, including applications to a multi-sensor navigation system and to the space shuttle's main engines. As one would hope, FDI is also important within the nuclear power industry. Singer et al. discuss the use of sequential statistical techniques in the analysis of the primary coolant pumping system in the EBR-II nuclear reactor. An expert system using pattern recognition and fuzzy inference techniques analyzes the statistical information to provide the fault detection. More recent work includes that of Visinski, et al. on fault detection thresholds based on dynamic system models. By including multiple redundant sensors in each servo system, as well as complete redundant servo systems, the knuckle was designed specifically for implementing and testing these types of algorithms.

In the current algorithm for the knuckle testbed, the servo control systems are assumed to be fully observable, deterministic, and linear time invariant. When an observable, accurate model exists, the FDI implementation uses parameter identification methods for detecting and, in many cases, isolating faults. The FDI algorithm also makes use of the currents in the DC servo system to determine whether enough torque can be generated to provide the motion desired. Threshold levels are set to check for deviations outside of the nominal values (which are determined experimentally) and any such deviations are classified as faults. The algorithm also filters "false alarms" generated by transient responses or noise levels outside the allotted error bands.

II-C. Digital Integrated Servo Controller (DISC)

The DISC is a very compact brushless DC servo controller that offers numerous features not contained in any single commercial system available today. Some of the features include: multiple sensor interfacing, compact 'smart' power electronics, fault tolerance, and high speed digital communications designed in a modular package. The features incorporated into each DISC allows for research into the use of distributed control applied to a modular robot. Distributed control can significantly reduce the amount of wires running through a structure since the DISCs digitally multiplex the signals locally. This reduction in wires is essential to the success of modular robotics and mechanical fault tolerance. The DISC contains four sub-modules: a sensor interface module, a communications module, a power interface module and a digital controller.

One of the DISC's advanced capabilities is its inherent fault tolerance. *Two DISCs connect in tandem with two motors to actuate a single degree of freedom.* In the event of a motor or sensor failure, a DISC can alert the system controller, and either shut itself down and allow operation to continue with only one motor, or try to isolate the fault and continue operation. Since a DISC uses parallel communication to talk to another DISC and it has control of the opposing Power Enable signal, two parallel DISCs act as a watchdog to each other. Thus, if a DISC were to fail, then the other DISC could detect the fault, alert the system controller, disable the faulty controller, disengage the clutch on the faulty controller, and continue operation with only one motor.

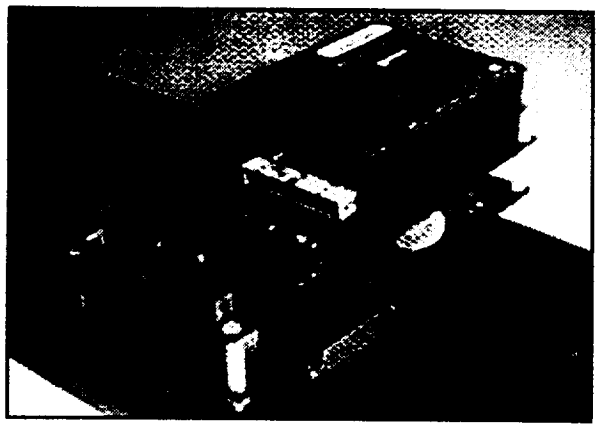

Figure 4. Photograph of the DISC

Property	Standard	DISC
Wiring	150 wires	13 wires
Speed	38 KBaud	10Mbaud
Modularity	none	4 Modules
Weight	3 lbs.	3 lbs.
Pwr. Density	15 W/in^3	15 W/in^3
Location	Remote	Collocated

Table 2. DISC vs. Standard Practice

Power Interface Module: The power interface controls the power to the actuator. It includes the power electronics and drivers, the clutch and brake control, and the current sensors. The DISC derives the motor commutation in software. In order to simplify the interface between the digital controller and the power interface, the power module uses a smart power electronic device. Smart power devices contain analog and/or digital circuitry in addition to the discrete power electronics. The device chosen for the DISCs generates the bias voltages for the high side discrete transistors as well as performing the lockout function for the input PWM logic.

Sensor Interface Module: The sensor module conditions and digitizes all external signals before passing them to the controller module. The module will read multiple sensors, including: a tachometer (16 bit resolution), three current sensors (12 bit resolution), a resolver (16 bit resolution), a torque sensor (12 bit resolution), an incremental encoder (16 bit resolution), two temperature sensors (8 bit resolution), a logic level Hall-effect sensor, an auxiliary +/- 5V signal (8 bit resolution) and an auxiliary +/- 10V signal (8 bit resolution). Each of the 12 and 16 bit analog signal lines has an anti-aliasing filter with a digitally adjustable cut-off frequency. As a precaution, the sensor module monitors the total actuator current with analog circuitry and if an over-current occurs, the analog circuitry shuts the system down.

The sensor interface module uses a five channel timing controller. Three channels function as a scheduler for sampling of the signals. The other two channels adjust the clock frequency of the anti-aliasing filters. The timer is software programmable.

Closed-Loop Controller Module: The closed-loop controller was purchased as an off-the-shelf component. The module is an Advanced Micro Device's SA-29200™ Demonstration Board. This card utilizes the Am29200 RISC microcontroller. The board has the following features: 512 KBytes of ROM, one MByte of DRAM, an RS-232 serial port, a JTAG port, two expansion connectors allowing full access to all processor signals, and a resident debugger. The system operates from a 5V power supply. The Am29200 is a 16 MHz, 32 bit integer processor with a ROM controller, a DRAM controller, an interrupt controller, a PIA controller, a 16 bit I/O port, a serial port, and a parallel port.

Communications Module: The communications module controls the information between the DISCs and the system controller. The difficulties inherent in electrical interface design for modular robots are primarily a result of the high number of wires that run throughout the robot. Most robots are controlled by monolithic system controllers. All data is brought to the system controller using separate conductors. As a result, every signal, sensor, and power wire for each actuator must be run throughout the entire robot to the system controller. For example, a Cincinnati Milacron Inc. T^3-776 industrial robot requires 24 wires for the tachometers, 54 wires for the resolvers, 18 wires for the brakes, 40 wires for powering the motors and cooling system, and 15 spare wires. This high number of wires (137) places difficult constraints on the design of connections within a modular robot that uses the centralized control scheme. For modular robots to be a viable alternative to monolithic robots the number of cables must be reduced. This can be achieved by using distributed control.

Distributed control is an alternative to external, centralized control that can drastically reduce the number of wires required in a robot. In distributed control each actuator has its own local intelligent controller that is mounted either adjacent to or directly inside the actuator. The local controller performs all necessary sensor processing and power conversion required for movement of the particular joint. The basic components of a local controller would include a central processing unit, a sensor interface, a power interface, and a communications interface.

The only external connections this local controller requires are for power and information. Since the local controller incorporates the power electronics interface, the power connections can be made to a common power bus that is used by all joints in the robot. Similarly, the information connections link the local controller to a simplified system controller through a serial digital communications bus. This communications bus carries all the information required to command each joint (where it should move and at what velocity torque). Depending on the types of power and communication buses the total number of wires can be less than ten. This potential drastic reduction in the number of wires required to run throughout a robot makes distributed control the method of choice for modular robotics.

III. Software

III-A. Multi-Criteria Decision Making for Configuration Management

This section discusses a method of redundancy resolution that uses local exploration to explicitly identify a set of options for the robot's motion. From this set, a decision making algorithm chooses one option as the next set-point command for the robot's servo controllers. The decision making algorithm can base its choice on any number of performance criteria. Simulated perturbations at the joint level drive the exploration. Eschenbach and Tesar developed the sequential filters method of decision making and applied it to the mechanism synthesis problem. They reported an example of the method reducing a design space of 60,000 to one of only 50. The following discussion details the application to redundant robots.

Perturbing the joint displacements a small amount, $\Delta\phi$, from their current values, $\underline{\phi}$, generates a set of local configuration options, $\underline{\hat{\phi}}$:

$$\underline{\hat{\phi}}: \underline{\hat{\phi}} = \underline{\phi} + \underline{\varepsilon}\Delta\phi,$$

where $\underline{\varepsilon}$ is an arbitrary sweep vector with all elements equal to ± 1 or 0. The vector of current displacement values, $\underline{\phi}$, is the base point for the perturbations. At the base point, $\underline{\varepsilon} = \underline{0}$. All other $\underline{\varepsilon}$ with elements equal to combinations of ± 1 and 0 generate points on the faces, edges, and vertices of an n-dimensional hypercube with n equal to the number of joints involved in the exploration. Figure 5. shows the hypercube for a robot with three degrees of redundancy. There are $2n$ points on the faces of the cube, 2^n points at the vertices, and 3^n points in all. Respectively, these are the simple, factorial, and exhaustive exploration patterns.

The six axis wrist approach is a method of satisfying the placement constraints on the robot's end effector while also significantly increasing the speed of the optimization. Essentially, the method satisfies the End-EFfector (EEF) placement constraints using a six-joint substructure of the robot's geometry. In essence, the method decouples the placement constraints on the robot's EEF from the optimization of the performance index. The name comes from an analogy with the three axis spherical wrist that decouples the rotational EEF placement constraints from the translational EEF placement constraints.

The method acts as a filter to eliminate options not satisfying the constraints on the placement of the robot's EEF. A series of three translations – P_X, P_Y, P_Z – and three rotations – R_X, R_Y, R_Z – will specify these constraints. The concatenation of the geometric transformations associated with these constraints generates a single transformation corresponding to the desired placement of the robot's EEF: ${}_{\text{desired}}\mathbf{T}$. The concatenation of the transformations associated with the robot's joint displacements – ϕ_0 to ϕ_n – and geometry (represented by the Denavit and Hartenberg parameters) must generate an equivalent transformation:

$${}^{o}_{n}\mathbf{T} = {}_{\text{desired}}\mathbf{T}$$

The formulation of the six-axis wrist approach proceeds as follows:

$${}^{0}_{n}\mathbf{T} = {}^{0}_{n-5}\mathbf{T}\ {}^{n-5}_{n}\mathbf{T},$$

and

$${}^{n-5}_{n}\mathbf{T} = {}^{0}_{n-5}\mathbf{T}^{-1}\ {}^{0}_{n}\mathbf{T}.$$

Given the general transformation, ${}^{n-5}_{n}\mathbf{T}$, the fully-constrained reverse position solution, ϕ_{n-5} to o_n, also satisfies ${}^{0}_{n}\mathbf{T}$ and thus ${}_{\text{desired}}\mathbf{T}$. Figure 6. depicts the geometry of these transformations.

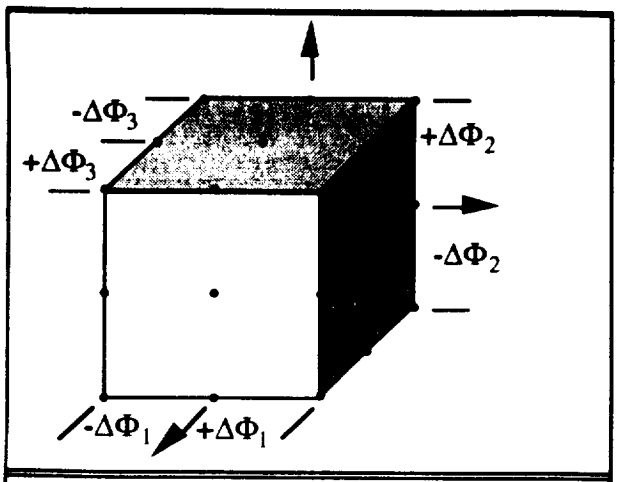

Figure 5. Hypercube for 3 Extra DOF

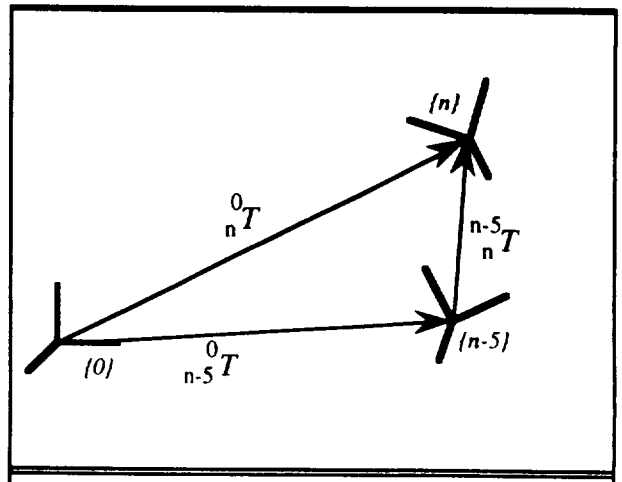

Figure 6. 6 Axis Wrist Transformations

Figure 7. shows a conceptual hyper-redundant robot with 21 DOF. NASA is studying this basic "serpentine" geometry for a number of space applications where the actuators will not have to support gravity loads, including: astronaut assist, tool site preparation, module change-out, tile and solar panel inspection, and tactile manipulation. A robot with this geometry can weave through obstacle-strewn environments and tolerate a number of faults while maintaining a large and dexterous workspace. Figure 8. shows a computer-generated trace of the robot following a straight EEF path. At the third frame in the trace, the robot experiences simulated failures in its 4th, 13th, 16th, and 18th joints simultaneously locking each joint. The redundancy resolution algorithm automatically reconfigures and maintains the EEF path.

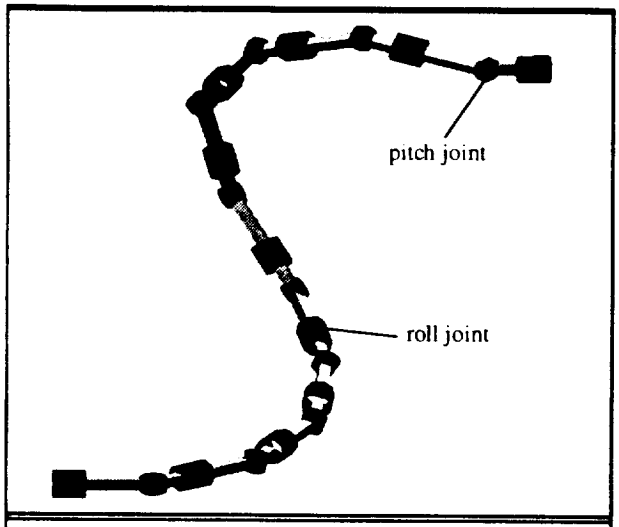

Figure 7. 21 DOF Serpentine Robot

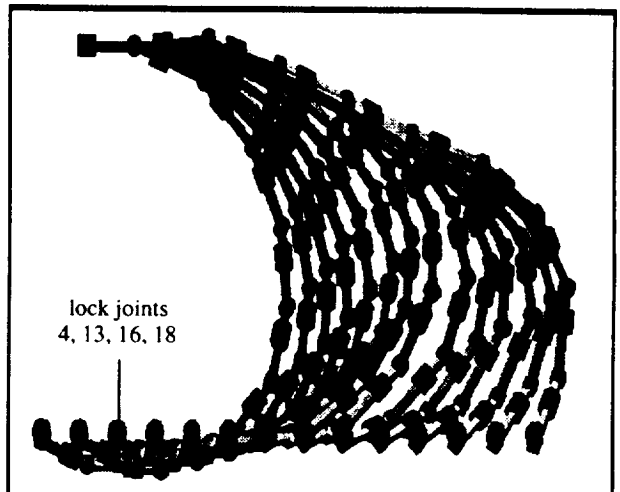

Figure 8. Maintains Path After Fault

III-B. Dual-Arm Control

Multiple arm robots represent the fourth and highest level in the fault-tolerant architecture. In the event of one arm failing, the extra arms could assume the task responsibilities. Fault tolerance at this level clearly demonstrates the need for active redundancies that provide increased capabilities as well as fault tolerance. The extra arms can provide additional task performance capabilities during normal operating conditions. A number of researchers have shown both experimental and theoretical work in cooperative manipulation using dual-arm robots. Notable examples include: manipulating single rigid objects single flexible objects, and manipulating two objects.

Figure 9. shows a graphic of a dual-arm robot with 17 DOF handling a thin plate. This application demands a balance of motion and force control representative of dual-arm operations. Multiple performance criteria form the basis for this balance. Figure 9. also includes the values of 5 performance criteria graphed against the percentage completion along the path. Figure 10. shows the actual robot (manufactured by the Robotics Research Corporation).

These criteria emphasize task-based performance indicators derived from the physical description of the manipulator. The origins of these criteria are from foundation activity in high speed mechanisms for production machinery. There, the issues of precision and modeling of complex non-linear structures forced the development of a geometric understanding for mechanical structures and how to represent them with efficient analytical tools. Thomas and Tesar showed that the concept of kinematic influence coefficients (used in systems with 1 DOF) were effective in spatial manipulator structures with N DOF.

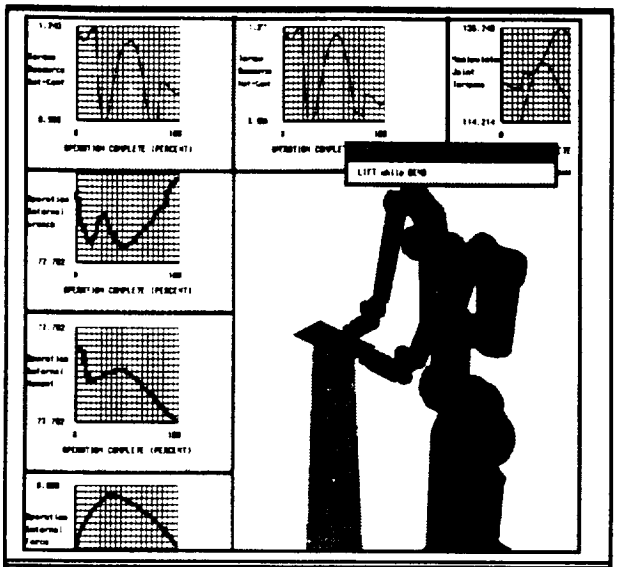

Figure 9. Robot Handling Thin Plate

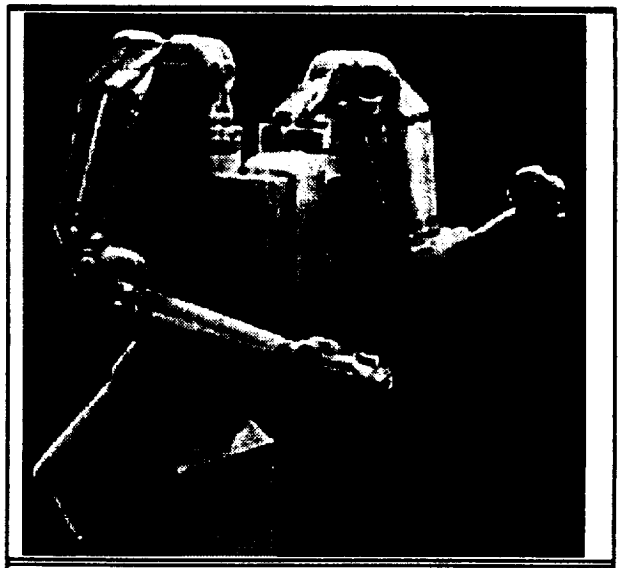

Figure 10. 17 DOF Dual-Arm Robot

IV. Theoretical

IV-A. Performance Criteria

Multiple performance criteria form the basis for configuration management in this work. These criteria emphasize task-based performance indicators derived from the physical description of the manipulator. The origins of these criteria are from foundation activity in high speed mechanisms for production machinery (Benedict and Tesar, 1978). There, the issues of precision and modeling of complex non-linear structures forced the development of a geometric understanding for mechanical structures and how to represent them with efficient analytical tools. Thomas and Tesar (1982) showed that the concept of kinematic influence coefficients (used in systems with 1 DOF) were effective in spatial manipulator structures with N DOF. An important development in this continuing work on performance criteria has been the association of performance criteria with the D&D tools the DAWM will use while performing its tasks. By choosing a tool, the operator will automatically scale and prioritize the criteria. This automatic process allows the use of multiple performance criteria without distracting the operator from the task at hand or consuming valuable time.

The criteria formulations emphasize efficiency and portability. With currently available computational hardware, decisions based on several of these criteria are possible in real-time. Given the rapid pace of

advancements in computational speed, it will soon be possible to employ the entire suite of performance criteria in a real-time decision making process. Table 3. lists the general categories of these performance criteria.

Table 3. General categories of performance criteria.

Category	Characteristics
constraint criteria	physical limitations
geometric	task independent
inertial	from dynamic models
compliance	design and operational issues
kinetic energy	content and distribution

The constraint criteria involve rapidly calculated elementary formulations. The robot's physical limitations form the basis for these criteria. These limitations restrict joint travels, joint speeds, joint accelerations, and joint torques. The Joint Range Availability (JRA) is representative and formulated as follows:

$$\text{JRA} = \sum_{i=1}^{n} \left[\frac{\left(\theta_i - \tilde{\theta}_i\right)^2}{\theta_{i\,max}^2} \right],$$

where θ_i is the joint displacement, $\tilde{\theta}_i$ is the mid-range displacement and $\theta_{i\,max}$ is the displacement at the joint limit. Throughout this report, θ_i corresponds to joint displacements. The JRA measures the joint's displacements away from their midpoints.

Geometric Criteria

The Jacobian matrix forms the basis for the geometric performance criteria. Table 4. lists some of the geometric performance criteria. These criteria are task independent and based only on the geometry of the robot, thus these criteria are formulated once for each robot with no need for reformulation if the task changes (Cleary and Tesar, 1990).

Table 4. Geometric performance criteria

Criterion	Symbol
singularity detection	η_σ
dexterity	η_δ
velocity transmission	$\eta_{v\chi}$
force and torque transmission	$\eta_{\tau\chi}$
Jacobian Frobenius Norm	η_Σ
change of singularity detection criterion	$\eta_{\Delta\sigma}$
change of dexterity criterion	$\eta_{\Delta\delta}$
EEF velocity-induced joint acceleration	$\eta_{\phi\alpha}$
joint velocity-induced EEF acceleration	$\eta_{v\alpha}$

The force transmission criterion represents the magnification that the joint torques will undergo in their transformation to the end-effector space. As such, it may be used to indicated configurations which generally require smaller joint torques to fulfill the required output forces. From the principle of virtual work, the joint torques required to drive the robot may be transferred to the end effector as

$$\tau = \boldsymbol{J}^T \boldsymbol{F},$$

where $\boldsymbol{J}$ is the manipulator Jacobian, $\boldsymbol{F}$ is the equivalent end-effector loads, and τ is the driving joint torques. The singular value decomposition (SVD) may be applied to the Jacobian as:

$$\boldsymbol{J} = \boldsymbol{U}\Sigma\boldsymbol{V}^T,$$

where the orthogonal matrices $\boldsymbol{U}$ and $\boldsymbol{V}$ contain the left and right singular vectors, and Σ is the diagonal matrix containing the singular values. Substituting the Jacobian and inverting the matrix of right singular vector results in:

$$\boldsymbol{V}^T\tau = \Sigma^T\boldsymbol{U}^T\boldsymbol{F},$$

where, because $\boldsymbol{V}$ is orthogonal, its inverse equals its transpose. Taking the 2-norm (Euclidean length) of $\boldsymbol{V}^T\tau$ yields:

$$\left\|\boldsymbol{V}^T\tau\right\|_2^2 = \sum_{i=1}^{r}\left(\sigma_i\left(\boldsymbol{U}^T\boldsymbol{F}\right)_i\right)^2,$$

where r is the rank of $\boldsymbol{J}$, and σ_i is $\boldsymbol{J}$'s i-th singular value. Because premultiplication by orthogonal matrices preserves the length of vectors, the left-hand side is simply the square of the 2-norm of the torque. Also, because the i-th element of $\boldsymbol{U}^T\boldsymbol{F}$ is a scalar, that product may be transposed and rewritten. With these modifications:

$$\|\tau\|_2^2 = \sum_{i=1}^{r}\left(\sigma_i\boldsymbol{F}^T\boldsymbol{U}_{:,i}\right)^2,$$

where $\boldsymbol{U}_{:,i}$ is the i-th column of $\boldsymbol{U}$. The end-effector force vector may now be decomposed into a magnitude, $\hat{F}$, and direction, $\{\boldsymbol{F}\}$.

$$\frac{\|\tau\|_2^2}{\hat{F}^2} = \sum_{i=1}^{r}\left(\sigma_i\left\{\boldsymbol{F}^T\right\}\boldsymbol{U}_{:,i}\right)^2.$$

Because the magnitude of a vector is its Euclidean length, we may conclude the development of the force transmission criterion, $\eta_{\tau\chi}$, by taking the square root of both sides and inverting as well.

$$\eta_{\tau\chi} = \frac{\|\boldsymbol{F}\|_2}{\|\tau\|_2} = \left[\sum_{i=1}^{r}\left(\sigma_i\{\mathbf{F}\}^T\mathbf{U}_{:,i}\right)^2\right]^{-1/2}.$$

Manipulator dexterity is the ability of the hand to move accurately and arbitrarily. Taken at the velocity level, a measure of this concept may be provided by the condition number of the manipulator Jacobian. The condition number is a numerical analysis tool which indicates the stability of a given transformation. Employed in this situation, the condition of the manipulator Jacobian indicates how error-prone the joint velocity vector (computed from the end-effector velocity through the inverse) will be. Perfect condition implies that any motion, regardless of direction, will be relatively free from numerical error. The

formulation of this criterion follows from the singular value decomposition of the manipulator Jacobian as shown above and is

$$\eta_\delta = \frac{\sigma_{min}}{\sigma_{max}},$$

where the σ's are the minimum and maximum singular values of J.

Inertial Criteria

Table 5. lists some of the inertial performance criteria. These criteria have their basis in dynamic models of forces and torques within the robot and are essential to the intelligent design and application of robots. The first four criteria deal with actuator torques. The next three criteria deal with the rate of change of torques. The rate of change of the actuator torque criterion, $\eta_{\Delta\tau}$, follows as:

$$\eta_{\Delta\tau} = \sqrt{\sum_{i=1}^{n}\left(\frac{\partial\lambda_{max}}{\partial\theta_i}\right)^2},$$

where λ_{max} is the maximum eigenvalue of the effective intertia matrix. This criterion measures how fast the robot can respond to torque and force demands. It is an especially important criterion because larger actuators or higher gear ratios can supply more torque, but both will slow the overall response of the robot to external disturbances. Consideration of the basic torque demands as well as its rate of change allows the intelligent allocation of the robot's torque resources for enhanced operation.

Table 5. Inertial performance criteria

Criterion	Symbol
dynamic coupling	η_ζ
actuator torque	η_τ
equivalent EEF forces	$\eta_{v\tau}$
EEF space actuator torque	$\eta_{v\phi\tau}$
change of actuator torque criterion	$\eta_{\Delta\tau}$
change of equivalent EEF forces criterion	$\eta_{\Delta v\tau}$
change of EEF space actuator torque crit.	$\eta_{\Delta v\phi\tau}$
velocity-induced actuator torque	$\eta_{v\tau}$
velocity induced equivalent EEF force	$\eta_{vv\tau}$
EEF velocity induced actuator torque	$\eta_{vv\phi\tau}$
GH norm	η_γ

Compliance Criteria

Table 6. lists the compliance performance criteria. The compliance criteria describe the robot's ability to perform precision operations under load. They also correspond to the vibratory modes of the robot. The compliance or stiffness of the manipulator is a chief concern in many tasks. When deflections are undesirable, the system stiffness criterion may be increased. From the generalized spring model of the manipulator,

$$F = [K]\Delta,$$

where F is the end-effector force vector, $[K]$ is the composite manipulator stiffness matrix, and Δ is the end-effector deflections. The arbitrary stiffness of the manipulator's configuration may be determined via the operator 2-norm of the stiffness matrix, which is its maximum eigenvalue, or the Frobenius (Euclidean) matrix norm, which is the square-root of the sum of the squares of all of the eigenvalues of $[K]$. A task-dependent criterion may also be defined in a manner similar to that of the force transmission as the structure of the linear equations is the same.

Table 6. Compliance performance criteria

Criterion	Symbol
oscillation	η_{ω}
system stiffness	η_{φ}
system potential energy	η_{ρ}
potential energy partition values	$\eta_{\rho\pi}$

The potential energy partition values, are particularly important compliance criteria. The potential energy partition values measure the distribution of compliance energy and how it changes as the robot moves. An unusually high compliance energy content in any part of the robot indicates a problem with the robot's design. Rapid changes in compliance energy indicate large local forces, which correspond to large actuator demands and decreased precision.

Kinetic Energy Criteria

Formulating the kinetic energy, KE, of a serial robot is straightforward:

$$\mathrm{KE} = \frac{1}{2}\dot{\theta}^{\mathrm{T}}\left[\mathbf{I}^{*}_{\theta\theta}\right]\dot{\theta},$$

where $\mathbf{I}^{*}_{\theta\theta}$ is the effective inertia matrix. This equation represents the entire kinetic energy content of the robot. In this formulation, the kinetic energy value depends on the joint speeds and therefore also depends on the task at hand. Van Doren and Tesar (1992) formulated a task-independent kinetic energy criterion, η_{κ}, as:

$$\eta_{\kappa} = \sqrt{\sum_{i=1}^{n} \lambda_i^2}\,.$$

The λ_i's are the eigenvalues of the effective inertia matrix.

Table 7. lists some of the kinetic energy performance criteria. These criteria address high-level issues represented in relatively simply formulations.

Table 7. Kinetic energy performance criteria

Criterion	Symbol
joint space kinetic energy	η_{κ}
EEF space kinetic energy	$\eta_{\upsilon\kappa}$
rate of change of joint space kinetic energy	$\eta_{\Delta\kappa}$
rate of change of EEF space kinetic energy	$\eta_{\Delta\upsilon\kappa}$
kinetic energy partition values	$\eta_{\kappa\pi}$

The rate of change of the kinetic energy, $\eta_{\Delta K}$, is an important criterion and formulated as follows:

$$\eta_{\Delta K} = \sqrt{\sum_{i=1}^{n} \left(\frac{\partial \eta_K}{\partial \theta_i} \right)^2}$$

Large changes in kinetic energy correspond to very large demands on actuator power. Very rapid changes in the kinetic energy represent shocks to the robot.

IV-B. Technical Reports

"***Design of a Three Degree-of-Freedom Robust Robotic Shoulder Module***", J. Fenwick and D. Tesar, The University of Texas at Austin, Report to U.S. Dept. of Energy, Grant DE-FG02-86NE37966, and NASA, Grant NAG 9-411, December 1990.

"***Design, Construction and Demonstration of Modular, Reconfigurable Robots***", R. Ambrose and D. Tesar, The University of Texas at Austin, Report to U.S. Dept. of Energy under Grant No. DE-FG02-86NE37966 and NASA-JSC under Grant No. NAG 9-411, August 1991.

"***Design and Prototype Development of Robot Actuator Modules***", J. Iaconis, D. Tesar, J. Geisinger, K. Shin, T. Ager, C. Pennington, M. Chu, and P. Varatharajan, The University of Texas at Austin, Report to Navy Explosive Ordnance Demolition Test Center, U.S. Dept. of Energy under Grant No. DE-FG02-86NE37966, and NASA under Grant No. NAG 9-411, December 1991.

"***A Roadmap for Standardized Sensor Technology in Modular, Reconfigurable Robots***", J. P. Nettle and D. Tesar, The University of Texas at Austin, Report to NASA under Grant No. NAG 9-411, U.S. Dept. of Energy under Grant No. DE-FG02-86NE37966, and Texas Higher Education Coordinating Board for Advanced Technology Program under Project No. 003658-156, December 1991.

"***Analysis of Redundantly Actuated Mechanisms with Applications to Design and Control of Advanced Robotic Systems***", B. J. Yi, R. A. Freeman, and D. Tesar, The University of Texas at Austin, Report to NASA under Grant No. NAG 9-411 and U.S. Dept. of Energy under Grant No. DE-FG02-86NE37966, January 1992.

"***An Applications-Based Assessment of Present and Future Robot Development***", M. S. Butler and D. Tesar, The University of Texas at Austin, Report to NASA under Grant No. NAG 9-411 and U.S. Dept. of Energy under Grant No. DE-FG02-86NE37966, May 1992.

"***Development and Demonstration of General, Real-Time Control Software for Robotic Manipulators***", R. Giddings and D. Tesar, The University of Texas at Austin, Report to U.S. Dept. of Energy under Grant No. DE-FG02-86NE37966 and NASA under Grant No. NAG 9-411, May 1992.

"***On the Design of Fault-Tolerant Robotic Manipulator Systems***", D. Sreevijayan and D. Tesar, The University of Texas at Austin, Report to NASA under Grant No. NAG 9-411 and Texas Higher Education Coordinating Board for Advanced Technology Program under Project No. 003658-156, June 1992.

"***Design of a Two DOF Gimbal Module for a Fault-Tolerance Test-Bed***", R. C. Walter and D. Tesar, The University of Texas at Austin, Report to NASA under Grant No. NAG 9-411 and U.S. Army Fully Funded Education Program, September 1992.

"***Reliability and Maintainability of Modular Robot Systems: A Roadmap for Design***", D. L. Schneider and D. Tesar, The University of Texas at Austin, Report to U.S. Air Force under Educational Services Agreement Number F33600-88-A-0264 and NASA under Grant No. NAG 9-411, May 1993.

"***Development of Real Time Operational Software for a Fault-Tolerance Testbed***", M. D. Rubin and D. Tesar, The University of Texas at Austin, Report to NASA under Grant No. NAG 9-411 and U.S. Dept. of Energy under Grant No. DE-FG02-86NE37966, June 1993.

"***Control Algorithms for Fault-Tolerant Robotic Manipulators***", Y. Ting, S. Tosunoglu, and D. Tesar, The University of Texas at Austin, Report to U.S. Dept. of Energy under Grant No. DE-FG02-86NE37966 and NASA under Grant No. NAG 9-411, December 1993.

"***The Design and Fabrication of a Two Degree of Freedom Knuckle Joint for a Fault Tolerant Test Bed***", M. Zung and D. Tesar, The University of Texas at Austin, Report to NASA under Grant No. NAG 9-411 and U.S. Dept. of Energy under Grant No. DE-FG02-86NE37966, February 1994.

"***Multicriteria Inverse Kinematics for General Serial Robots***", R. N. Hooper and D. Tesar, The University of Texas at Austin, Report to NASA under Grant No. NAG 9-411 and U.S. Dept. of Energy under Grant No. DE-FG02-86NE37966, May 1994.

"***Developing Mechanical Design Procedures for Lightweight Stiff Actuator Module***", K. Shin and D. Tesar, The University of Texas at Austin, Report to U.S. Dept. of Energy under Grant No. DE-FG02-86NE37966 and to NASA under Grant No. NAG 9-411, August 1994.

IV-C. List of Participants in Program

Those Who Received M.Sc. Degrees

T. Ager
R. Ambrose
J. Geisinger
C. Pennington
J. Nettle
M. Butler
R. Giddings
D. Sreevijayan
R. Walter
M. Rubin
M. Zung
R. Hooper
M. Chu

Those Who Received Ph.D. Degrees

R. Ambrose
J. Geisinger
B. Yi
R. Giddings
D. Sreevijayan
D. Schneider
Y. Ting
R. Hooper
K. Shin
M. Chu (Dissertation due)
B. Nowak (Dissertation due)

Staff and Faculty Involved

Prof. D. Tesar, Program Director
Dr. R. Hooper, Chief Scientist (1994-97)
Dr. S. Tosunoglu, Chief Scientist (1985-94)
Prof. R. Freeman, Faculty Associate